# Structural and optical properties of europium doped zirconia single crystals fibers grown by laser floating zone

M. R. N. Soares, C. Nico, M. Peres, N. Ferreira, A. J. S. Fernandes, T. Monteiro,[a] and F. M. Costa
*Department of Physics, Laboratory I3N, University of Aveiro, Campus Universitário de Santiago, 3810-193 Aveiro, Portugal*

(Received 2 September 2010; accepted 16 November 2010; published online 10 January 2011)

Yttria stabilized zirconia single crystal fibers doped with europium ions were developed envisaging optical applications. The laser floating zone technique was used in order to grow millimetric high quality single crystal fibers. The as-grown fibers are completely transparent and inclusion free, exhibiting a cubic structure. Under ultraviolet (UV) excitation, a broad emission band appears at 551 nm. The europium doped fibers are translucent with a tetragonal structure and exhibit an intense red emission at room temperature under UV excitation. The fingerprint transition lines between the $^5D_0$ and $^7F_{J(0-4)}$ multiplets of the $Eu^{3+}$ ions are observed with the main emission line at ~606 nm due to $^5D_0 \rightarrow {}^7F_2$ transition. Photoluminescence excitation and wavelength dependent the photoluminescence spectra confirm the existence of different $Eu^{3+}$ optical centers. © *2011 American Institute of Physics*. [doi:10.1063/1.3527914]

## I. INTRODUCTION

The properties of zirconia based materials have been extensively modified by the addition of stabilizing oxides, allowing the development of this ceramic material envisaging technological applications. For these applications, the two most important structures are the high-temperature ones (cubic and tetragonal) which are unstable in bulk forms at room temperature (RT).[1–3] The addition of $Y_2O_3$ and rare-earth (RE) to the $ZrO_2$ is known to enhance the structural stability in both elements cubic and tetragonal phases, depending on the dopant amount and processing temperature.[4,5] Besides to the role of the $RE^{3+}$ ions as stabilizers, their optical activation constitutes an opportunity to explore the zirconia-based material in the photonics area. In fact, the visible and infrared transitions of several lanthanide ions in bulk, microstructured, and nanostructured zirconia polymorphs processed by different routes have been exploited by different research groups for potential applications as solid state lighting and displays.[6–23] Indeed, associated with the high energy bandgap, the low phonon energy resulting from the small stretching frequency (470 $cm^{-1}$) exhibited by $ZrO_2$ foresees a high yield of the intra-$4f^n$ transitions from the RE doped zirconia,[14–16,21–25] a suitable host material for optical applications such as optical active waveguides.

Among the mentioned lanthanide ions, trivalent europium is known to give rise to the intense orange-red luminescence. This is mainly due to $^5D_{0,1} \rightarrow {}^7F_{J(0-4)}$ multiplet transitions in several insulator and wide band gap semiconductor hosts like GaN-based materials,[26,27] for which a highly efficient $Eu^{3+}$ related electroluminescent device was recently reported.[28] Regardless the synthesis technique and polytype in zirconia host doped with europium ions, optical activation was achieved, allowing the observation of the $^5D_{0,1} \rightarrow {}^7F_J$ transitions mainly in nano/micro polycrystalline samples.[6,7,14,18,19,21,23]

In order to take advantage of the potentialities of $Eu^{3+}$ ions for optical applications in zirconia hosts, a deep knowledge of its behavior in single crystal material is required. However, it is well known that the growth of zirconia single crystal is a hard task, considering its high melting temperature. The laser floating zone (LFZ) is a suitable method to grow zirconia single crystals due to laser local heating and absence of crucible. Though, internal cracks tend to develop due to the high residual thermal stress when temperature gradients are not controlled.[29] This growth technique was previously used to grow $ZrO_2$ single crystals doped with $Er^{3+}$ and $Pr^{3+}$ (Refs. 12 and 13) but, and as far as we know, single crystals fibers of $Eu^{3+}$ doped zirconia were never studied up to now.

In this work, the LFZ fabrication technique was used to grow high quality europium doped zirconia single crystal fibers with millimetric diameters at high growth rates. The spectroscopic characteristics of the lanthanide ion in the fibers were analyzed by photoluminescence (PL) and PL excitation (PLE) between 14 K and RT. The presence of different $Eu^{3+}$-related centers is discussed.

## II. EXPERIMENTAL DETAILS

The single crystal zirconia fibers were grown by the LFZ technique, using rod precursors for both feed and seed materials prepared by cold extrusion. These rods were obtained by mixing the initial powders, zirconia with 8 mol % of $Y_2O_3$ (Tosoh Corporation) and 3 mol % $Eu_2O_3$ (Aldrich) with polyvinyl alcohol (0.1 g/ml, Merck) in order to obtain a slurry that was further extruded into cylindrical rods with diameters of 1.75 mm.

The LFZ equipment comprises a 200 W $CO_2$ laser (Spectron) coupled to a reflective optical setup producing a

[a]Electronic mail: tita@ua.pt.

 

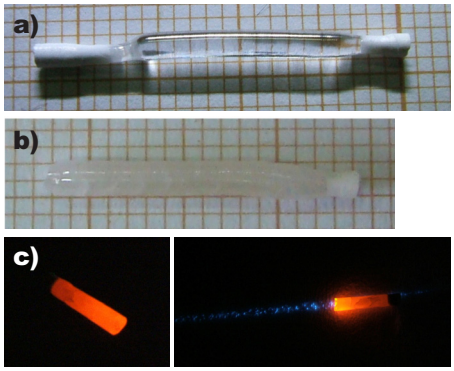


FIG. 1. (Color online) (a) Single crystal fibers of YSZ pulled at 40 mm/h; (b) europium doped fibers pulled at 40 mm/h; and (c) europium doped fibers under 325 nm laser excitation at RT.

circular crown-shaped laser beam in order to obtain a floating zone configuration with a uniform radial heating. Single crystal fibers with diameters in the range of 1.5–2 mm and 20–30 mm in length were grown at 40 and 100 mm/h in air at atmospheric pressure.

Fiber microstructure and phase development were characterized by scanning electron microscopy (Hitachi S4100) with energy dispersive spectroscopy (EDS) on polished surfaces of longitudinal fiber sections. The structural characterization was accomplished by x-ray diffraction (XRD) experiments (PANalytical X'Pert PRO) and ultraviolet (UV)-Raman spectroscopy (Horiba Jobin Yvon HR800) in backscattering configuration excited by the 325 nm line of a He–Cd laser (Kimmon IK Series).

Steady state PL measurements were carried out between 14 K and RT using the same He–Cd laser, a 457 nm line of a Melles–Griot laser and a 1000 W Xe arc lamp coupled to a monochromator as excitation sources. The used excitation energies correspond to energies below the tetragonal $ZrO_2$ bandgap which was predicted by theoretical models as 6.4 eV.[30] For the PLE measurements, the emission monochromator was set to the $Eu^{3+}$ emission lines and the excitation wavelength was scanned up to 240 nm. The spectra were corrected to the lamp and optics.

## III. RESULTS AND DISCUSSION

The single crystal fibers of yttria stabilized $ZrO_2$ (YSZ) resulted to be completely transparent, uniform, and inclusion free, as seen in Fig. 1(a). In this picture, it is still possible to see the precursor rods localized at the fiber extremities. The feed and seed rods appear white and opaque due to its polycrystalline nature. The picture shown in Fig. 1(a) presents the typical aspect of YSZ fibers grown at different pulling rates (40 and 100 mm/h). The addition of 8 mol % $Y_2O_3$ stabilized the crystallization of the cubic structure, as confirmed by XRD (not shown) and Raman spectroscopy, Fig. 2(a). In fact, UV-Raman measurements performed in backscattering geometry corroborate the presence of a distorted cubic fluorite-type structure ($O_h^5$) with the $Y^{3+}$ ions located in the $Zr^{4+}$ sites, being the charge compensation mechanisms assured by the presence of oxygen vacancies. For the YSZ fiber, a dominant vibrational mode corresponding to the first-order Raman-active mode at the Γ point ($T_{2g}$ symmetry) is observed at ~600 $cm^{-1}$,[31,32] as shown in Fig. 2(a). Indeed, the breakdown of the $\vec{q}=0$ selection rule due to the anion sublattice disorder leads to a spectrum that resembles the one-phonon density of states.[32]

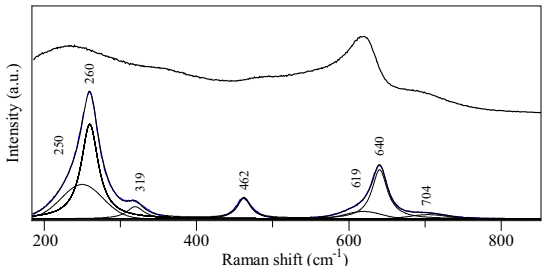


FIG. 2. (Color online) Raman spectra of: (a) YSZ (cubic); and (b) europium doped YSZ fibers (tetragonal).

The addition of 3 mol % $Eu_2O_3$ to the initial precursor of YSZ resulted in translucent fibers, Fig. 1(b) with a tetragonal structure, as revealed by XRD (not shown), and Raman spectroscopy, Fig. 2(b). The cubic to tetragonal phase transition induced by the dopant incorporation is clearly revealed by the presence of the active Raman modes around 250, 319, 462, 619, and 640 $cm^{-1}$. An expected peak near 146 $cm^{-1}$ cannot be seen since it falls within the filter region that extends to ~200 $cm^{-1}$. An unassigned weak contribution at 704 $cm^{-1}$ is also present. This band appears in other works but its low signal intensity renders it almost negligible.[33] A group theory analysis for the tetragonal zirconia structure predicts that optical and acoustic phonon modes at the Γ point of the Brillouin zone have the symmetries $A_{1g}+2B_{1g}+3E_g+2A_{2u}+3E_u+B_{2u}$.[34] Among these symmetries, the $A_{1g}$, $2B_{1g}$, and $3E_g$ are Raman active. Concomitantly, the vibrational frequencies found in the present work are in fair agreement with those recently assigned as $A_{1g}$ (270 $cm^{-1}$), $B_{1g}$ (318 $cm^{-1}$), $E_g$ (458 $cm^{-1}$), $B_{1g}$ (602 $cm^{-1}$), and $E_g$ (648 $cm^{-1}$), by visible (514.5 nm) polarized Raman spectroscopy.[34]

The morphological analysis of the fiber longitudinal sections, Figs. 3(a) and 3(b), reveals uniform surface without

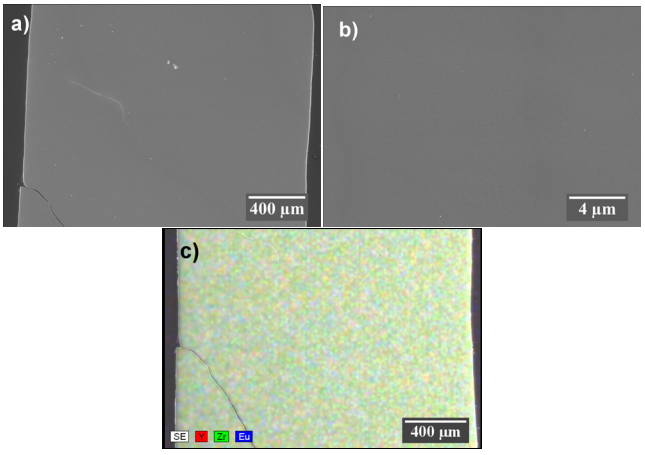


FIG. 3. (Color online) SEM micrographs of longitudinal sections of an europium doped fiber pulled at 40 mm/h: (a) general view; (b) high magnification; and (c) EDS maps of Zr, Y, and Eu concentration along the fiber diameter.

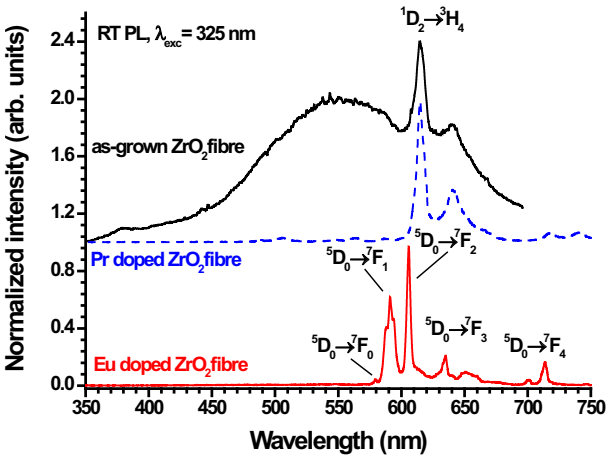


FIG. 4. (Color online) RT PL spectra of undoped and europium doped fibers pulled at 40 mm/h under 325 nm He–Cd laser excitation. For comparison the RT PL spectrum of a praseodymium doped fiber pulled at 40 mm/h is also shown (dashed line).

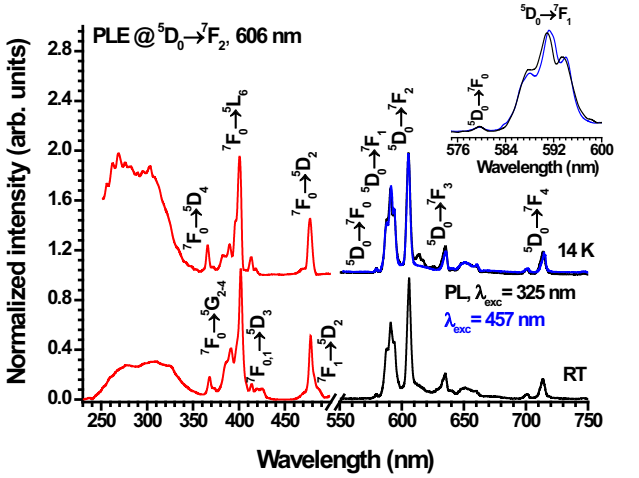


FIG. 5. (Color online) Comparison between the 14 K and RT PL and PLE spectra of the europium doped fiber.

grain boundaries or second phases, confirming its monophasic and monocrystalline character. The EDS analysis shows an europium uniform distribution along the fiber diameter and axis, Fig. 3(c).

The RT PL spectra of both undoped and europium doped fibers are shown in Fig. 4. Under UV excitation, the undoped transparent fiber exhibits an unstructured broad emission band peaked at 551 nm (2.25 eV). Broad unstructured deep level recombination in the yellow/orange spectral region has been observed in the different $ZrO_2$ polymorphs and assigned to F-type defects, involving the oxygen vacancy and their complexes.[35–38] Overlapped with the F-type emission band, the as-grown cubic stabilized $ZrO_2$ fibers show an additional emission in the red region with pronounced maxima at 614 nm (2.02 eV) and 641 nm (1.93 eV). These maxima were previously observed in polycrystalline YSZ and were attributed to the intraionic recombination of a lanthanide ion present as a contaminant in the samples.[35] As the peak position and spectral shape of the observed lines match those of the transition between the $^1D_2$ and $^3H_4$ multiplets of the $Pr^{3+}$ ion,[10,13,17,39] it is likely that in our as-grown samples praseodymium ions could be present as precursors contaminants. Actually, praseodymium doped tetragonal zirconia fibers were further produced and characterized, confirming the above assumption, as shown by the dashed line in Fig. 4.

The RT luminescence of the europium doped fibers under UV excitation clearly evidences the fingerprint transition lines between the $^5D_0$ and $^7F_{J(0-4)}$ multiplets of the $Eu^{3+}$ ions (Fig. 4). Europium ions are known to be spectroscopic probes in different hosts due to the simplest structure of its $^{2S+1}L_J$ multiplets with nondegenerate first excited and ground levels, $^5D_0$ and $^7F_0$, respectively. In addition, the number of Stark components and intensity ratio of the $^5D_0 \rightarrow {}^7F_J$ transitions are typically used for acquiring information about the symmetry at the $Eu^{3+}$ site. The main emission line from the europium doped $ZrO_2$ fiber occurs in the red region at ~606 nm, corresponding to the electric dipole allowed $^5D_0 \rightarrow {}^7F_2$ transition. Given the absence of inversion symmetry, the spectra display additional lines, ascribed to the following transitions: ~579 nm, the strictly forbidden $^5D_0 \rightarrow {}^7F_0$; ~591 nm, the parity allowed magnetic dipole induced $^5D_0 \rightarrow {}^7F_1$; ~635 nm, a weak mixed character $^5D_0 \rightarrow {}^7F_3$; ~714 nm, the electric dipole allowed $^5D_0 \rightarrow {}^7F_4$. The intense RT $Eu^{3+}$ luminescence under UV excitation is undoubtedly observed by naked eye as shown in Fig. 1(c).

Dexpert-Ghys *et al.*,[6] in their work on yttria-doped zirconia ceramics, have shown the PL spectra of $Eu^{3+}$ ions in $ZrO_2$ samples with different monoclinic, tetragonal and cubic polymorphs. Our data shown in Fig. 4 corroborate their results for the europium emission peak positions and intensity ratio of the $^5D_0 \rightarrow {}^7F_J$ transitions in tetragonal $ZrO_2$, according to our XRD and Raman identification.

Figure 5 shows a comparison between the PL (14 K and RT) and PLE spectra of the europium doped fiber. For both temperatures, under 325 nm excitation, the $^5D_J \rightarrow {}^7F_J$ multiplet transitions occur at the same position, meaning that the emission comes only from the first excited state, $^5D_0$, even at RT. The number of transitions between the nondegenerate $^5D_0$ and $^7F_0$ multiplets is usually used to estimate the number of $Eu^{3+}$ sites in a crystalline lattice. For instance, this was the case observed for other oxide host fibers grown by the LFZ method.[40] The spectra shown in Figs. 4 and 5 evidence the presence of a $^5D_0 \rightarrow {}^7F_0$ transition at ~579 nm. The appearance of this emission, together with a threefold Stark splitting of the $^5D_0 \rightarrow {}^7F_1$, means that the emitting $Eu^{3+}$ ions must lay at a lower symmetry than the expected tetragonal $D_{4h}$ for the ion in a cation substitutional site. On the other hand due to local changes in the crystal field, the full width at half maximum (FWHM) of the line (~5.3 meV) is rather large when compared with those of the $^5D_0 \rightarrow {}^7F_0$ transitions in other oxides fibers grown by the same method. As an example, in $Ta_2O_5$ fibers, the FWHM is lower than <1 meV.[40] The width of the $^5D_0 \rightarrow {}^7F_0$ transition in $ZrO_2$ doped samples grown by different routes was also studied by other authors.[6,7,18] Particularly, site-selective spectroscopy measurements performed on the $^5D_0 \rightarrow {}^7F_0$ transition[6,7] eliminated inhomogeneous broadening, revealing different $Eu^{3+}$-centers in the samples. In order to investigate if LFZ grown doped fibers exhibit multiple europium related optical

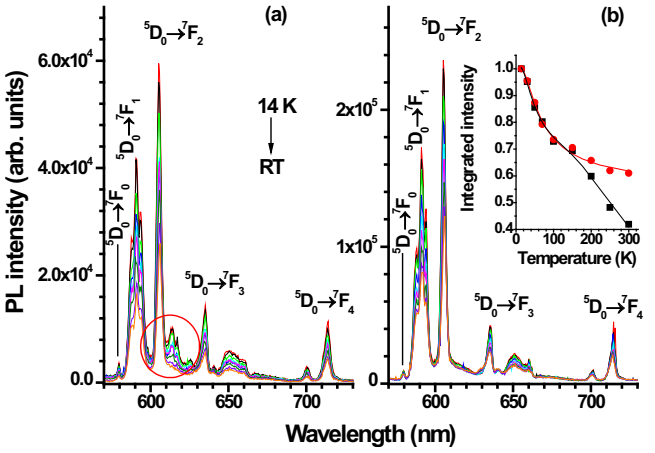


FIG. 6. (Color online) Temperature dependence of the $Eu^{3+}$ luminescence for two excitation wavelengths, 325 nm (a) and 457 nm (b). The inset depicts the evolution of the integrated intensity of the overall luminescence with temperature.

centers, PLE (Fig. 5) and wavelength dependent excitation (Figs. 5 and 6) measurements were performed. The 14 K and RT PLE spectra monitored at the $^5D_0 \rightarrow {}^7F_2$ transition (606 nm) display the excitation paths for the observation of the $Eu^{3+}$ luminescence. The narrower lines are ascribed to several intra-$4f^6$ transitions between the ground state $^7F$ to the excited states $^5D$, $^5L$, and $^5G$ multiplets, as labeled in Fig. 5. In addition to the sharper lines, the excitation spectrum of the $Eu^{3+}$ luminescence shows two overlapping absorption bands with maxima at ~310 nm and ~270 nm. In wide band gap hosts and apart the parity forbidden $f \rightarrow f$ transitions, the excitation spectra of the RE ions typically exhibit broad absorption bands due to the parity allowed interconfigurational $4f^n \rightarrow 4f^{n-1}5d$ and charge transfer (CT) transitions.[41,42] The CT bands, also of interconfigurational nature, involve for instance the promotion of the ligand electrons to the metal ion and usually occur in the UV region.[24,41–44] For the case of $Eu^{3+}$ in oxide hosts, the promotion of an electron from a ground state configuration $4f^6$ to the lowest $4f^55d$ level occurs in the UV and vacuum UV spectral region.[41–44] On the other hand, the CT transitions are known to occur at longer wavelengths than the $f-d$ transitions and their peak positions are known to decrease in energy with larger average distance of the surrounding anions.[43,44] As the CT states locate at lower energies than those of the $Eu^{3+}$ $4f^55d$ levels we believe that the two observed excitation bands with maxima at 310 and 270 nm (Fig. 5) correspond to two different CT transitions as also detected in other zircon based compounds.[24] Considering the relative intensity of the absorption bands in the PLE spectra, the $Eu^{3+}$ luminescence from the $^5D_0$ level is preferentially populated by CT mechanisms rather than the intra-$4f^6$ $Eu^{3+}$ excited levels. A comparison between the PL spectra obtained with excitation in the CT region and in the intra-$4f^6$ excited states (above the $^5D_2$ level) can be observed in Figs. 5 and 6. In both cases, the transitions intensity ratio is comparable but small shifts in the peak position of the $^5D_0 \rightarrow {}^7F_J$ transitions can be identified, as shown in the inset of Fig. 5. Moreover, exciting the samples via the CT band leads to the appearance of additional lines in the $^5D_0 \rightarrow {}^7F_2$ spectral region, as highlighted in Fig. 6, suggesting the presence of different $Eu^{3+}$ optical centers in accordance with the observation by PLE of different Eu–O distances.

The temperature dependence of the $Eu^{3+}$ luminescence was studied for two excitation wavelengths, 325 nm and 457 nm (Fig. 6), corresponding to the excitation via the CT band and $^5D_2$ energy level, respectively. The temperature dependence of all the $^5D_0 \rightarrow {}^7F_J$ integrated intensity is shown in the inset of Fig. 6. The nonradiative de-excitation mechanisms of $Eu^{3+}$-related centers are similar up to 150 K. However, for higher temperatures, a steeper decrease in the PL intensity is observed when the fibers are excited via the CT band indicating additional nonradiative de-excitation paths. Exciting the samples in the CT band, the RT PL intensity accounts for ~40% of the low temperature luminescence. With the excitation on the $^5D_2$ multiplet, a lower decrease in the integrated intensity is observed, ~60% of the low temperature intensity being still observed at RT. The identification of the different $Eu^{3+}$ optical centers with their influence on the de-excitation mechanisms of the overall RT europium luminescence under different excitation conditions could help improving the excitation efficiency of this oxide host in thermal barrier coatings.[45]

## IV. CONCLUSIONS

Single crystal fibers ($\varnothing \approx 1.5-2$ mm and $L \approx 20-30$ mm) of 8 mol % YSZ and europium doped $ZrO_2$ were successfully grown by the LFZ technique at high pulling rates (40 and 100 mm/h). The undoped crystals exhibit cubic structure and are completely transparent while the doped ones are translucent with a tetragonal structure.

Under UV excitation, the undoped cubic fibers reveal an unstructured broad emission band at 551 nm (2.25 eV) together with an additional emission in the red region with maxima at 614 nm (2.02 eV) and 641 nm (1.93 eV), attributable to the transition between the $^1D_2$ and $^3H_4$ multiplets of the $Pr^{3+}$ ion, possibly a contaminant in the raw powders.

The $Eu^{3+}$ doped YSZ grown fibers display an intense light guiding effect of the red emission at RT under UV excitation. Moreover, these fibers clearly evidence the fingerprint transition lines between the $^5D_0$ and $^7F_{J(0-4)}$ multiplets of the $Eu^{3+}$ ions, being the main emission line in red region at ~606 nm due to the electric dipole allowed $^5D_0 \rightarrow {}^7F_2$ transition. The PLE study has shown that $Eu^{3+}$ ions are preferentially populated via the CT bands rather than the intra-$4f^6$ configuration. Nevertheless, under the former excitation conditions, the detected $^5D_0 \rightarrow {}^7F_J$ luminescence at RT corresponds to 40% of its value at low temperature when compared with the 60% observed with intraconfigurational excitation, meaning that additional nonradiative paths occur under the CT excitation. The presence of different $Eu^{3+}$ optical centers was discussed based on the observation of the two excitation CT bands and wavelength dependent PL spectra.

## ACKNOWLEDGMENTS

The authors acknowledge FCT for the financial funding from PTDC/CTM/66195/2006 project. M. Peres thanks FCT for the Ph.D. grant, Grant No. SFRH/BD/45774/2008.

[1]A. Ghosh, S. Sabharwal, A. K. Suri, B. T. Rao, and T. R. R. Mohan, Adv. Appl. Ceram. **107**, 170 (2008).
[2]C. Laberty-Robert, F. Ansart, C. Deloget, M. Gaudon, and A. Rousset, Ceram. Int. **29**, 151 (2003).
[3]G. Bernard-Granger, N. Monchalin, and C. Guizard, Scr. Mater. **57**, 137 (2007).
[4]D. W. Liu, C. H. Perry, and R. P. Ingel, J. Appl. Phys. **64**, 1413 (1988).
[5]T. H. Etsell and S. N. Flengas, Chem. Rev. **70**, 339 (1970).
[6]J. Dexpert-Ghys, M. Faucher, and P. Caro, J. Solid State Chem. **54**, 179 (1984).
[7]H. Yugami, A. Koike, M. Ishigame, and T. Suemoto, Phys. Rev. B **44**, 9214 (1991).
[8]R. I. Merino, V. M. Orera, R. Cases, and M. A. Chamarro, J. Phys.: Condens. Matter **3**, 8491 (1991).
[9]C. K. Loong, G. K. Liu, M. Ozawa, and S. Suzuki, J. Alloys Compd. **250**, 352 (1997).
[10]B. Savoini, J. E. Muñoz Santiuste, and R. González, Phys. Rev. B **56**, 5856 (1997).
[11]R. I. Merino, V. M. Orera, O. Povill, W. Assmus, and E. E. Lomonova, J. Phys. Chem. Solids **58**, 1579 (1997).
[12]F. S. Vicente, A. C. Hernandes, A. C. Castro, M. F. Souza, M. R. B. Andreeta, and M. S. Li, Radiat. Eff. Defects Solids **147**, 77 (1998).
[13]F. S. De Vicente, A. C. Hernandes, A. C. Castro, M. F. Souza, M. R. B. Andreeta, and M. S. Li, Radiat. Eff. Defects Solids **149**, 153 (1999).
[14]R. Reisfeld, M. Zelner, and A. Patra, J. Alloys Compd. **300–301**, 147 (2000).
[15]A. Patra, C. S. Friend, R. Kaoor, and P. N. Prasad, J. Phys. Chem. B **106**, 1909 (2002).
[16]E. De la Rosa-Cruz, L. A. Diaz-Torres, P. Salas, R. A. Rodríguez, G. A. Kumar, M. A. Meneses, J. F. Mosiño, J. M. Hernández, and O. Barbosa-Garcia, J. Appl. Phys. **94**, 3509 (2003).
[17]F. Ramos-Brito, M. Garcia-Hipólito, R. Martínez-Martínez, E. Martínez-Sánchez, and C. Falcony, J. Phys. D: Appl. Phys. **37**, L13 (2004).
[18]L. Chen, Y. Liu, and Y. Li, J. Alloys Compd. **381**, 266 (2004).
[19]Z. W. Quan, L. S. Wang, and J. Lin, Mater. Res. Bull. **40**, 810 (2005).
[20]E. De la Rosa, D. Solis, L. A. Díaz-Torres, P. Salas, C. Angeles-Chavez, and O. Meza, J. Appl. Phys. **104**, 103508 (2008).
[21]F. Trivinho-Strixino, F. E. G. Guimarães, and E. C. Pereira, Mol. Cryst. Liq. Cryst. **485**, 766 (2008).
[22]F. Ramos-Brito, C. Alejo-Armenta, M. García-Hipólito, E. Camarillo, J. Hernandez, H. Murrieta, and C. Falcony, Opt. Mater. **30**, 1840 (2008).
[23]G. Cabello, L. Lillo, C. Caro, G. E. Buono-Core, B. Chornik, and M. A. Soto, J. Non-Cryst. Solids **354**, 3919 (2008).
[24]D. Van der Voort and G. Blasse, Chem. Mater. **3**, 1041 (1991).
[25]M. M. Trexler, D. Zhang, L. Kelly, and J. Sample, J. Mater. Res. **25**, 500 (2010).
[26]T. Monteiro, C. Boemare, M. J. Soares, R. A. S. Ferreira, L. D. Carlos, K. Lorenz, R. Vianden, and E. Alves, Physica B **308–310**, 22 (2001).
[27]A. J. Steckl, J. H. Park, and J. M. Zavada, Mater. Today **10**, 20 (2007).
[28]A. Nishikawa, T. Kawasaki, N. Furukawa, Y. Terai, and Y. Fujiwara, Appl. Phys. Express **2**, 071004 (2009).
[29]L. Tong, J. Cryst. Growth **217**, 281 (2000).
[30]B. Králik, E. K. Chang, and S. G. Louie, Phys. Rev. B **57**, 7027 (1998).
[31]J. Cai, C. Raptis, Y. S. Raptis, and E. Anastassakis, Phys. Rev. B **51**, 201 (1995).
[32]M. Ishigame and E. Yoshida, Solid State Ionics **23**, 211 (1987).
[33]D. Gazzoli, G. Mattei, and M. Valigi, J. Raman Spectrosc. **38**, 824 (2007).
[34]T. Merle, R. Guinebretiere, A. Mirgorodsky, and P. Quintard, Phys. Rev. B **65**, 144302 (2002).
[35]E. D. Wachsman, N. Jiang, C. W. Frank, D. M. Mason, and D. A. Stevenson, Appl. Phys. A: Mater. Sci. Process. **50**, 545 (1990).
[36]S. E. Paje and J. Llopis, Appl. Phys. A: Mater. Sci. Process. **57**, 225 (1993).
[37]N. G. Petrik, D. P. Taylor, and T. M. Orlando, J. Appl. Phys. **85**, 6770 (1999).
[38]H. Nakajima and T. Mori, J. Alloys Compd. **408–412**, 728 (2006).
[39]J. F. Fidelus, S. Yatsunenko, M. Godlewski, W. Paszkowicz, E. Werner-Malento, and W. Lojkowski, Scr. Mater. **61**, 415 (2009).
[40]C. P. L. Rubinger, L. C. Costa, M. Macatrão, M. Peres, T. Monteiro, F. M. Costa, N. Franco, E. Alves, B. Z. Saggioro, M. R. B. Andreeta, and A. C. Hernandes, Appl. Phys. Lett. **92**, 252904 (2008).
[41]G. Blasse, *Handbook on the Physics and Chemistry of Rare Earths* (Elsevier Science, North- Holland Physics Publishing, 1979), Vol. 4, p. 34.
[42]G. Blasse and B. C. Grabmaier, *Luminescent Materials* (Springer, Berlin, 1994).
[43]H. E. Hoefdraad, J. Solid State Chem. **15**, 175 (1975).
[44]P. Dorenbos, J. Lumin. **111**, 89 (2005).
[45]M. M. Gentleman and D. R. Clarke, J. Surf. Sci. Technol. **200**, 1264 (2005).